NONEQUILIBRIUM THERMODYNAMIC MODEL OF THE RAT PROXIMAL TUBULE EPITHELIUM

ALAN M. WEINSTEIN
Department of Physiology and Biophysics, Cornell University Medical College, and Rogosin Kidney Center, The New York Hospital, New York, New York 10021

ABSTRACT The rat proximal tubule epithelium is represented as well-stirred, compliant cellular and paracellular compartments bounded by mucosal and serosal bathing solutions. With a uniform pCO_2 throughout the epithelium, the model variables include the concentrations of Na, K, Cl, HCO_3, H_2PO_4, HPO_4, and H, as well as hydrostatic pressure and electrical potential. Except for a metabolically driven Na-K exchanger at the basolateral cell membrane, all membrane transport within the epithelium is passive and is represented by the linear equations of nonequilibrium thermodynamics. In particular, this includes the cotransport of Na—Cl and Na—H_2PO_4 and countertransport of Na—H at the apical cell membrane. Experimental constraints on the choice of ionic conductivities are satisfied by allowing K—Cl cotransport at the basolateral membrane. The model equations include those for mass balance of the nonreacting species, as well as chemical equilibrium for the acidification reactions. Time-dependent terms are retained to permit the study of transient phenomena. In the steady state the energy dissipation is computed and verified equal to the sum of input from the Na—K exchanger plus the Gibbs free energy of mass addition to the system. The parameter dependence of coupled water transport is studied and shown to be consistent with the predictions of previous analytical models of the lateral intercellular space. Water transport in the presence of an end-proximal (HCO_3-depleted) luminal solution is investigated. Here the lower permeability and higher reflection coefficient of HCO_3 enhance net sodium and water transport. Due to enhanced flux across the tight junction, this process may permit proximal tubule Na transport to proceed with diminished energy dissipation.

INTRODUCTION

The proximal tubule reabsorbs the bulk of the plasma filtrate created at the glomerulus. In the mammalian kidney, this is a briskly transporting epithelium, and the large volume of water transported is powered by metabolically-driven solute reabsorption (Windhager et al., 1959; Morel and Murayama, 1970). The actual forces that drive this water from tubular lumen to peritubular capillaries remain an area of controversy. In part, this controversy derives from the high water permeability of this epithelium, with the consequence that the net forces required are small, and their measurement is technically difficult. Nevertheless, the available data indicate that the observed water transport cannot totally be ascribed to the establishment of a transepithelial osmotic gradient (with a tubule lumen hypotonic to plasma). Indeed, along the length of the proximal tubule, the tubule fluid osmolality was found to be isosmotic with plasma (Gottschalk, 1963), or at best, only slightly hypotonic (Bishop et al., 1979; Green and Giebisch, 1982).

For the mammalian proximal tubule the rationalization of the forces of water reabsorption is further complicated by the changing ionic composition of the luminal fluid as one moves from early to late proximal tubule. Due to acidification of tubule contents there is progressive depletion of luminal bicarbonate. Although cryoscopically nearly isosmotic to plasma, the late proximal tubule solution is higher in chloride and lower in bicarbonate than the peritubular plasma. This ionic asymmetry can provide a force for net water reabsorption if the osmotic reflection coefficient for bicarbonate is greater than that for chloride. Available data indicate that this is likely for proximal tubule, both from measurements of reflection coefficients (Ullrich, 1973) and measurements of water flux across perfused proximal tubules with an imposed transtubular ionic gradient (Schafer et al., 1975, Neumann and Rector, 1976). Nevertheless, these forces are operative only in the later segment of the proximal tubule and still may provide for only a fraction of the net water reabsorption. One is led, therefore, to consider mechanisms of intraepithelial solute-linked water transport. Intraepithelial solute-solvent coupling has been well-documented in such tissues as gallbladder and small intestine, that, like the proximal tubule, can sustain large volume flows between isosmotic media. Like the proximal tubule, this volume flow is proportional to the rate of metabolically driven salt transport. It is generally believed that in these epithelia the lateral intercellular space is the locus of intraepithelial solute-solvent coupling. Salt transport into the interspace creates a region of hypertonicity that pulls water across highly permeable cell membranes. Small elevations of hydrostatic pressure within the interspace propel this solu-

tion outward across the basement membrane and into the serosal bathing medium. The feasibility of such a system has been demonstrated by elaboration of mathematical models that can simulate the water transporting parameters of the gallbladder epithelium (Weinstein and Stephenson, 1981*a*).

Several mathematical models have been used in connection with proximal tubule water transport. Sackin and Boulpaep (1975) and Huss and Marsh (1975) published single solute, nonelectrolyte models of the lateral intercellular spaces of the proximal tubule of *Necturus* and of the rat. Although these models allowed for solute diffusion within the interspace, the solutions of the model equations showed no significant solute gradients. Based on this work, and subsequent confirmation both numerically and analytically in gallbladder models (Weinstein and Stephenson, 1981*b*), we consider the interspace as a single, well-stirred compartment. Sackin and Boulpaep (1975) used this simplification to formulate a model of *Necturus* proximal tubule that included the cell as a well-stirred compartment and that recognized the two ionic species, Na^+ and Cl^-. This permitted the inclusion of electrical potential as a model variable and the incorporation of model parameters obtained from electrical experiments. Huss and Marsh (1975) and, subsequently, Huss and Stephenson (1979) in a single solute cell and interspace model, included a compliance law for the lateral intercellular space. This represented more realistically the observed changes in interspace dimensions in response to variations in pressure. Schafer et al. (1977), modeling the lateral intercellular space of the rabbit proximal tubule, were the first to incorporate the bicarbonate species in their model, and in particular, to formally consider the effect of chloride-bicarbonate asymmetry on water transport. Their boundary conditions, however, included an infinitely permeable channel basement membrane, and thus implicitly denied the possibility of substantial intraepithelial solute-solvent coupling. The intraepithelial coupling of solute and water fluxes will be considered here in detail. Finally, note the elegant model by Wang and Deen (1980) of CO_2 transport across the rat proximal tubule cell. The model predicted only a small CO_2 gradient across the tubule, comparable with that which was subsequently measured (3.3 mm Hg across the early proximal tubule, by Gennari et al. [1982]). In this investigation a uniform pCO_2 has been assumed throughout the cell and interspace.

The model of proximal tubule presented here is comprised of well-stirred, compliant, cellular and intercellular compartments bounded by infinite luminal (mucosal) and peritubular (serosal) bathing media. The model solutes are Na^+, K^+, Cl^-, HCO_3^-, $HPO_4^=$ $H_2PO_4^-$, and H^+. Within the cell there is an anionic impermeant species that may also serve as a proton buffer. In the Model Equations section the time-dependent mass balance equations are formulated for this system in a manner that allows for interconversion of species according to pH equilibria. In the Membrane Transport Equations section the transport laws for each species across the individual membranes within the model system are shown. Except for a metabolically driven Na^+-K^+ exchange at the basolateral cell membrane, all ion movement is given by the linear relations of nonequilibrium thermodynamics. At the apical membrane of the proximal tubule cell, the movement of Cl^-, $H_2PO_4^-$, and H^+ are all coupled to the movement of Na^+. In this section a condition is derived for the degrees of coupling of these species to insure that the apical cell membrane is a "passive" structure in the thermodynamic sense. The Choice of Parameters and Numerical Methods section displays the parameters chosen for the model, taken to achieve compatibility with what is known of the rat proximal convoluted tubule. Here the arguments will be made for choosing basolateral K^+-Cl^- cotransport as a mechanism for rationalizing the net fluxes of these species with the electrical resistance of the membrane.

The steady-state solution of the model equations and some of the "permeabilities" of the model epithelium are presented in the Steady State Open-Circuited Epithelium section and compared with data from the rat. Utilizing the thermodynamic formulation of the membrane transport equations, the energy dissipation of the model epithelium is calculated and related to the free energy of hydrolysis of ATP. In view of the interconversion of reacting species there is no simple mass conservation that can be verified for these species. What is done, however, is that the relatively small free-energy input from mass entry into the system is added to the energy input from the Na^+-K^+ exchanger and this sum is shown equal to the energy dissipation. Conservation of energy is verified for each steady-state problem to within the limits of accuracy of the computer.

The final section explores the water transporting properties of the model epithelium. The parametric dependence of uphill water transport and of isotonic transport for this acidifying epithelium are shown to be in qualitative agreement with results previously derived for the gallbladder epithelium. Isotonic transport is found to be crucially dependent upon cell membrane water permeability, but little influenced by interspace basement membrane solute permeability. Intraepithelial solute-solvent coupling, however, is enhanced both by high cell membrane water permeability and by low interspace basement membrane solute permeability. When such coupling is significant, the cell membrane water permeability will be substantially greater than the epithelial water permeability measured with an imposed osmotic gradient. The effect of luminal bicarbonate depletion on water transport and proton transport is calculated for several values of pCO_2. In these circumstances it is shown that in the presence of anion asymmetry the paracellular pathway may assume increased importance as a route for Na reabsorption. This paracellular reabsorption occurs with a substantially reduced energy dissipation per mole of sodium transported.

It suggests a selective energetic advantage for the low resistance shunt pathway in this segment of the nephron.

GLOSSARY

Subscripts

Compartments

M	luminal (mucosal) solution
S	peritubular (serosal) solution
I	intracellular compartment
E	lateral intercellular space or extracellular channel

Membranes

MI	apical cell membrane
ME	tight junction
IE	lateral cell membrane
IS	basal cell membrane
ES	channel basement membrane.

Intensive Variables

α refers to any compartment subscript; t, time.

$\psi_\alpha(t)$	electrical potential, mV
$p_\alpha(t)$	hydrostatic pressure, mm Hg
$C_{i\alpha}(t)$	concentration of solute i, mmol/cm^3 i = 1, Na^+; i = 2, K^+; i = 3, Cl^-; i = 4, HCO_3^-; i = 5, $HPO_4^=$; i = 6, $H_2PO_4^-$; i = 7, H^+.
C_l	cell impermeant species osmolality, mOsM/cm^3
C_{Buf}, C_{HBuf}	cell buffer concentrations, unprotonated and protonated forms, mmol/cm^3
$\mu_{i\alpha}(t)$	electrochemical potential of species i, J/mmol.

Membrane Properties

β refers to any membrane subscript.

$L_{p\beta}$	water permeability, cm/s · mm Hg
$\sigma_{i\beta}$	reflection coefficient of solute i
$L_{ij\beta}$	thermodynamic coefficient for solutes i and j, (mmol)^2/J · s · cm^2
$q_{ij\beta}$	degree of coupling between solutes i and j, dimensionless
$g_{i\beta}$	partial conductance of solute i, $(\Omega cm^2)^{-1}$
$P_{i\beta}$	permeability of solute i, cm/s
A_β	area, cm^2/cm^2 epithelium.

Flows[1]

β refers to any membrane subscript, α to any compartment.

$J_{v\beta}(t)$	volume flow, ml/s · cm^2
$J_{i\beta}(t)$	flux of solute i, mmol/s · cm^2
$J_{i\beta}^{act}$	metabolically driven transport of solute i
$\Phi_{i\beta}$	energy dissipation due to flux of solute i, J/s · cm^2
$G_{i\alpha}$	free energy input due to mass entry, J/s · cm^2.

Geometric Parameters

α refers to cell or channel.

$L(t)$	cell (channel) height, cm
S	cell circumference, cm/cm^2 epithelium (mean)
V_α	volume, cm^3/cm^2 epithelium
ν_E	channel compliance, (mm Hg)$^{-1}$
ν_L	cell height compliance, (mm Hg)$^{-1}$.

[1]Flows in the direction away from the lumen are positive; flows from cell to channel are positive.

Constants

z_i	valence of solute i
z_l	impermeant species valence
pK_C	pK for the bicarbonate-carbonic acid pair
pK_P	pK for the phosphate buffer
pK_B	pK of cell buffer
RT	product of gas constant and temperature
F	faraday.

Derived Variables

C_R	ratio of transepithelial osmotic flux to water flow (reabsorbate concentration), mOsM/ml
C_o	reference osmolality
γ	osmotic coupling coefficient (C_o/C_R)
C_M^*	mucosal equilibrium osmolality, deviation from reference for which reabsorbate osmolality is equal to luminal osmolality (serosa at reference)
C_S^*	serosal equilibrium osmolality, deviation from reference for which reabsorbate osmolality is equal to peritubular osmolality (mucosa at reference)
$\hat{C}$	strength of transport, maximum osmotic gradient against which volume can be transported.

MODEL EQUATIONS

The model configuration is depicted schematically in Fig. 1 and the notation used for the model variables and parameters is indicated in the Glossary. There are four compartments to the system representing the luminal or mucosal (M) solution, the peritubular or serosal (S) solution, the intracellular compartment (I), and the lateral intercellular space or extracellular compartment (E). Within each compartment, α, we consider the hydrostatic pressure, p_α, the electrical potential, ψ_α, and the concentrations, $C_{i\alpha}$, where i = 1, . . ., 7 refers to Na^+, K^+, Cl^-, HCO_3^-, $HPO_4^=$, $H_2PO_4^-$, and H^+, respectively. The cell also contains impermeant species with osmotic activity, C_l, and a concentration of unprotonated buffering sites, C_{Buf}, and protonated buffering sites C_{HBuf}. The volumes of the cell and channel are designated V_α, α = I, E. In the model calculations, the cell and channel pressure, voltage, and ionic concentrations, and the cell buffer concentrations are unknowns of the system, thus comprising 20 variables. In the open-

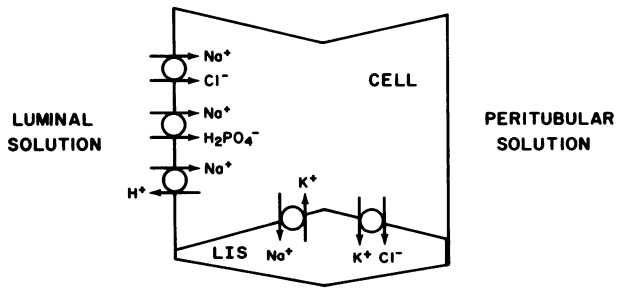

FIGURE 1 Schematic representation of the proximal tubular cell and lateral intercellular space (LIS). At the apical cell membrane there is cotransport of Na^+ with Cl^- and with $H_2PO_4^-$, as well as Na^+/H^+ countertransport. At the lateral cell membrane there is K^+-Cl^- cotransport and a metabolically driven Na^+/K^+ exchanger.

circuited epithelium the transepithelial potential, ψ_M, is an additional variable. Otherwise all luminal and peritubular variables are specified, as well as the epithelial pCO_2.

In reference to Fig. 1, there are five membranes in the model system, namely, the apical cell membrane (subscripted MI), the basal cell membrane (IS), the lateral cell membrane (IE), the tight junction (ME), and the channel basement membrane (ES). Across each membrane, β, there is a volume flow, $J_{v\beta}$, and for each species, i, a solute flux $J_{i\beta}$. Thus, per unit time, the net efflux from the cellular compartment, Q_{iI}, may be written $Q_{iI} = J_{iIS} + J_{iIE} - J_{iMI}$, and efflux from the channel, Q_{iE}, is $Q_{iE} = J_{iES} - J_{iIE} - J_{iME}$.

The mass conservation equations for the model may now be formulated. Any volume loss of cell or channel (α = I, E) must result from net volume efflux

$$-\frac{d}{dt}V_\alpha = Q_{v\alpha}. \tag{1}$$

Similarly for the nonreacting species (i = 1, 2, 3), any solute loss must result from net solute efflux

$$-\frac{d}{dt}(C_{i\alpha}V_\alpha) = Q_{i\alpha}. \tag{2}$$

The reacting species must be considered separately. Within the cell there is conservation of total buffer

$$\frac{d}{dt}[V_I(C_{Buf} + C_{HBuf})] = 0. \tag{3}$$

For both cell and channel the loss of total phosphate must be balanced by the efflux of total phosphate

$$-\frac{d}{dt}[V_\alpha(C_{5\alpha} + C_{6\alpha})] = Q_{5\alpha} + Q_{6\alpha}. \tag{4}$$

Finally, the net creation of protons within the cell must be equal to the new buffer created within the cell in the form of bicarbonate, basic phosphate, or impermeant base

$$\frac{d}{dt}(V_IC_{7I}) + Q_{7I} = \left[\frac{d}{dt}(V_IC_{4I}) + Q_{4I}\right] + \left[\frac{d}{dt}(V_IC_{5I}) + Q_{5I}\right] + \frac{d}{dt}(V_IC_{Buf}). \tag{5}$$

A similar equation, without impermeant buffer, applies to the interspace.

The reacting species are assumed to be always at pH equilibrium. This yields the additional model equations

$$pH_\alpha - 6.1 = -\log C_{7\alpha} - 6.1 = \log\frac{C_{4\alpha}}{0.03 \cdot pCO_2} \tag{6}$$

$$pH_\alpha - 6.8 = -\log C_{7\alpha} - 6.8 = \log\frac{C_{5\alpha}}{C_{6\alpha}}. \tag{7}$$

For the cell, a similar type of relation is assumed to exist for the impermeant buffer

$$-\log C_{7I} - pK_B = \log\frac{C_{Buf}}{C_{HBuf}}. \tag{8}$$

Within both cell and channel, electroneutrality is preserved at each moment in time. With z_i the valence of species i, this means that in the channel

$$\sum_{i=1}^{7} z_iC_{iE} = 0 \tag{9}$$

and in the cell

$$\sum_{i=1}^{7} z_iC_{iI} + z_IC_I - C_{Buf} = 0, \tag{10}$$

where z_I is the valence of the osmotically active impermeant species. Eqs. 1–10 constitute the system of 20 equations corresponding to the 20 unknown intensive variables within the epithelial compartments. When the open-circuited preparation is to be modeled, the condition of zero net current is represented by equation

$$\sum_{i=1}^{7} z_i(J_{iME} + J_{iMI}) = 0. \tag{11}$$

For the mass balance Eqs. 1–5 the cell and channel volumes are expressed as linear functions of the pressures within each compartment. This approach is, of necessity, empirical, but is intended to eliminate the unrealistically large swings in intraepithelial hydrostatic pressures that may occur in models of fixed geometry. In the gallbladder, for example, Spring and Hope (1978) have shown that even small increments in serosal hydrostatic pressure may result in substantial increases in the volume of the lateral intercellular space. As in previous gallbladder models, the area of the channel basement membrane, A_{ES}, has been written in the form of a compliance relation of the cell and channel pressure difference

$$A_{ES} = A^\circ_{ES}[1 + \nu_E(P_E - P_I)]. \tag{12}$$

The channel flares linearly to its widest bulge, $b \cdot A_{ES}$, at the midpoint and then tapers linearly to a fixed tight junction area, A_{ME}. The volume of the channel is then

$$V_E = \frac{L}{4}(A_{ES} + 2b \cdot A_{ES} + A_{ME}), \tag{13}$$

where L is the height of both cell and channel, i.e., epithelial thickness. The cell height itself has been written as a function of the intracellular pressure and, as in previous models, is of the form

$$L = L^\circ[1 + \nu_L(P_I - P_M)]. \tag{14}$$

With this type of a compliance relation (and a relatively large ν_L), intracellular pressures remain small in the model calculations reported in this work. Note that the cell height is also the epithelial volume (cm^3/cm^2) so that the cell volume is calculated as the difference of epithelial volume and channel volume, V_E.

MEMBRANE TRANSPORT EQUATIONS

To solve the system of equations developed in the preceding section, it remains to specify the membrane fluxes in terms of the intensive variables. Fromter (1974), following Sauer (1973), has presented a set of relations in a form convenient for physiological problems. For a system of n solutes, the volume flow, J_v, across a membrane is

$$J_v = L_p\Delta p - L_pRT\sum_{i-1}^{n}\sigma_i\,\Delta C_i, \tag{15}$$

where Δp and ΔC represent pressure and concentration differences across the membrane of interest. L_p is the water permeability of the membrane, σ_i is the ionic reflection coefficient, and RT the product of the gas constant and absolute temperature of the system. For solutes, the flux J_i, is written as the sum of three terms, representing convective, diffusive, and metabolically driven transport

$$J_i = (1 - \sigma_i)\overline{C}_iJ_v + \sum_{j-1}^{n} L_{ij}\Delta\mu_j + J_i^{act}. \tag{16}$$

Here $\Delta\mu_j$ is the electrochemical potential difference of the solute across the membrane

$$\Delta\mu_j = RT\Delta\ln C_j + z_jF\Delta\psi \tag{17}$$

and $\overline{C}_i$ is a mean membrane concentration of species i

$$\overline{C}_i = \frac{\Delta C_i}{\Delta\ln C_i}. \tag{18}$$

The coefficient, L_{ij}, relates the flux of species i to the electrochemical driving force on species j. When i $\neq$ j this permits a representation of coupled solute fluxes. From thermodynamic theory, mutual interactions (near equilibrium) are equal, so that $L_{ij} = L_{ji}$ (Sauer, 1973).

For subsequent considerations it will be useful to relate the coefficients of Eq. 16 to the common measures of ion permeation, the partial conductance, and the permeability. When ion–ion interaction is absent ($L_{ij} = 0$ for i $\neq$ j), a change in voltage, $\Delta\psi$, will induce a change in the current carried by species i of the amount, $\Delta I_i = z_iF\Delta J_i = z_i^2F^2L_{ii}\Delta\psi$. The partial conductance, g_i, is therefore

$$g_i = z_i^2F^2L_{ii}, \tag{19}$$

and the total electrical resistance of this membrane is just

$$R = \left[\sum_{i-1}^{n} g_i\right]^{-1}. \tag{20}$$

The change in solute flux in response to a small change in solute concentration is $\Delta J_i = L_{ii}RT\Delta\ln C_i = L_{ii}RT(\Delta C_i/\overline{C}_i)$, so that the permeability, P_i, is

$$P_i = \frac{L_{ii}RT}{\overline{C}_i}. \tag{21}$$

In the model calculations presented the coefficients, L_{ij}, have been taken as constant parameters. Their selection is indicated in the following section.

For the passive transport of dilute solutions across membranes, in the steady state, Sauer (1973) has identified the dissipation of free energy, Φ, as the product of the flows and conjugate driving forces used in Eqs. 15 and 16

$$\Phi = J_v\left(\Delta P - RT\sum_{i-1}^{n}\Delta C_i\right) + \sum_{i-1}^{n} J_i\Delta\mu_i. \tag{22}$$

The energy input into the system from metabolically driven transport is just the sum of terms

$$\sum_{i-1}^{n} J_i^{act}\,\Delta\mu_i$$

for each of the membranes for which $J_i^{act} \neq 0$. In this model of proximal tubule, such active transport terms pertain only to the lateral cell membrane, and for the sodium and potassium species. There is, however, an additional input of free energy from mass addition to the system. In the normal mode of transport, solutes and water are continually added to the luminal solution and removed from the peritubular solution. When these solutions differ, either in ion concentration or in electrical potential, a net transfer of free energy occurs. For the luminal solution, for example, this energy input, G_M, would be equal to the sum

$$G_M = (J_{vME} + J_{vMI})\left(P_M - \sum_{i-1}^{7} RTC_{iM}\right) + \sum_{i-1}^{7}(J_{iME} + J_{iMI})\mu_{iM}.$$

Within the cell and channel the net creation of a species ($Q_{i\alpha} > 0$) is an additional source of free energy. Thus for the cell, for example, the energy input, G_I, is

$$G_I = \sum_{i-1}^{7} Q_{iI}\mu_{iI}.$$

Note these energy calculations are valid only for the steady state problems, in which the compartment volumes are constant. In the model calculations presented the free energy input from mass addition is usually a tiny fraction of the total energy dissipation of the system. Nevertheless, it must be included to verify conservation of energy.

For a passive membrane, that is, without metabolically driven transport, there is an additional constraint in the choice of the coefficients L_{ij}. According to the second law of thermodynamics, any choice of driving forces ($\Delta\mu_i$) must result in a set of flows (J_i) in such a manner that the energy dissipation

$$\Phi = \sum_{i-1}^{n} J_i\Delta\mu_i = \sum_{i-1}^{n}\sum_{j-1}^{n} L_{ij}\Delta\mu_j\Delta\mu_i$$

is positive. In other words, the matrix $L = (L_{ij})$ must not only be symmetric, it must also be positive definite. This poses a special problem for the selection of coefficients for the apical cell membrane. Since in the present work this membrane is to be a passive membrane, one must have a means of selecting positive definite matrices. In the remainder of this section a simple method for such parameter selection is presented. It utilizes the fact that for this

membrane all ion coupling is presumably with a single species, i.e., Na^+.

To formulate this result recall the "degree of coupling" utilized by Essig and Caplan (1968) in their analysis of the matrix of resistive coefficients. For ease of notation, denote $L_j = L_{jj}$, and define the degree of coupling, q_j, of species j to Na (species 1) by

$$q_j = \frac{L_{1j}}{\sqrt{L_1 L_j}}. \tag{23}$$

When q_j is positive a transmembrane driving force for sodium results in cotransport of species j; conversely a negative q_j represents countertransport. Then for the matrix, L, of the form

$$L = \begin{bmatrix} L_1 & \cdots & L_{1j} & \cdots & L_{1n} \\ \vdots & \ddots & & & \\ & & & & \\ L_{1j} & & L_j & & 0 \\ \vdots & & & \ddots & \\ & 0 & & & \\ L_{1n} & & & & L_n \end{bmatrix}$$

Proposition. L is positive definite if and only if $L_j > 0, j = 1, \ldots, n$ and

$$\sum_{j-2}^{n} q_j^2 \le 1. \tag{24}$$

It is straightforward to verify that

$$\det(L) = \left(1 - \sum_{j-2}^{n} q_j^2\right)\left(\prod_{i-1}^{n} L_i\right). \tag{25}$$

Then if L is positive definite $L_i > 0$ for each $i = 1, n$ so that the second factor on the right is positive. Further, if L is positive definite then det (L), the product of its eigenvalues, must also be positive. This means that the first factor on the right is positive.

Now suppose Eq. 24 is true; consider the quadratic form

$$\begin{aligned} \langle X, LX \rangle &= \sum_{j-1}^{n} L_j X_j^2 + 2\sum_{j-2}^{n} L_{1j} X_1 X_j \\ &= L_1\left[X_1^2 + 2X_1 \sum_{j-2}^{n} \frac{L_{1j}}{L_1} X_j\right] + \sum_{j-2}^{n} L_j X_j^2 \\ &= L_1\left[X_1^2 + 2X_1 \sum_{j-2}^{n} \frac{L_{1j}}{L_1} X_j + \left(\sum_{j-2}^{n} \frac{L_{1j}}{L_1} X_j\right)^2\right] \\ &\quad + \left[\sum_{j-2}^{n} L_j X_j^2 - \left(\sum_{j-2}^{n} \frac{L_{1j}}{\sqrt{L_1}} X_j\right)^2\right] \\ &= L_1\left[X_1 + \sum_{j-2}^{n} \frac{L_{1j}}{L_1} X_j\right]^2 \\ &\quad + \left[\sum_{j-2}^{n} L_j X_j^2 - \left(\sum_{j-2}^{n} q_j \sqrt{L_j} X_j\right)^2\right]. \end{aligned}$$

But by the Cauchy-Schwartz inequality

$$\left(\sum_{j-2}^{n} q_j \sqrt{L_j} X_j\right)^2 \le \left(\sum_{j-2}^{n} q_j^2\right)\left(\sum_{j-2}^{n} L_j X_j^2\right)$$

and, using Eq. 24

$$\left(\sum_{j-2}^{n} q_j \sqrt{L_j} X_j\right)^2 \le \sum_{j-2}^{n} L_j X_j^2.$$

Thus the difference of these terms is nonnegative and the quadratic form is positive, as desired.

As a consequence of this proposition, the actual task of choosing parameters for the apical cell membrane is that of choosing the straight coefficients, L_j, and then the degrees of coupling, q_j, so that Eq. 24 is satisfied. The coefficients L_{ij} are then back-calculated according to Eq. 23. The parameter selections are indicated in the following section.

CHOICE OF PARAMETERS AND NUMERICAL METHODS

Unless otherwise specified the parameters used in the model calculations are those displayed in Table I. Wherever possible, parameter choices have been made so as to be concordant with experimental data from the rat proximal tubule. Although for many of the parameters there are no direct experimental determinations, their choice has been dictated by the desire to achieve cellular concentrations and potential (Table II) as well as whole epithelial fluxes and permeabilities (Table III) compatible with the rat proximal tubule epithelium.

The apical cell membrane area, amplified by microvilli, has been taken equal to the lateral cell membrane area, amplified by membrane infolding, both 45 cm^2/cm^2 epithelium. The equality of these two membrane areas has been demonstrated in rabbit proximal convoluted tubule by Welling and Welling (1975) who found an amplification factor of 20 or 36, depending on either a basal or apical epithelial reference area. The unit membrane water permeability has been taken at 3.8×10^{-4}ml/s · cm^2OsM. This is only slightly larger than the estimate of the water permeability of the rabbit proximal straight tubule peritubular membrane of 2.9×10^{-4}ml/s · cm^2 OsM by Gonzalez et al. (1982) and within the range of unit water permeabilities for red cell membranes (Macey, 1979). The cell membranes have been taken to have reflection coefficients of 1.0, so that all solute species exert their full osmotic effect. This is compatible with the data of Gonzalez et al. (1982) for proximal tubule and Persson and Spring (1982) for gallbladder cells. The channel basement membrane water permeability used is that of Welling and Grantham (1972) for rabbit proximal tubule basement membranes, and their finding of basement membrane solute reflection coefficients of zero is also incorporated into the model. The water permeability of the tight junction is, at present, unknown for any epithelium. In the

present calculations, the water permeability of the junction was chosen so as to be equal to the transcellular water permeability. Solute reflection coefficients were then selected to achieve agreement with the whole epithelial reflection coefficients determined for the rat proximal tubule (Table III).

The apical membrane sodium permeability is the major determinant of the net transepithelial sodium flux. This value was selected, therefore, so as to yield the desired flux. Spring and Giebisch (1977) have shown that the basolateral sodium pump may be thought of as a high capacity transporter that increases its activity in a linear fashion in response to increases in the intracellular sodium concentration. An empirical pump law has been incorporated into the model (Table I) with constants chosen to achieve an intracellular sodium concentration comparable with that obtained by electron probe analysis (Thurau et al., 1981). Note that in all the model calculations it is the concentrations of the ionic species that are employed. Obviously, in the mass balance equations, the concentrations are necessary to specify the compartmental solute contents, but ionic activities should be employed in calculating the driving forces across membranes. The activity coefficients, relating cell ion activity to ion concentration, are, unfortunately, unknown. The use of concentrations in these calculations introduces, implicitly, the assumption that activity coefficients for each compartment are equal. The acceptability of this assumption has been suggested by Spring and Kimura (1979) but cannot be considered secure (Khuri, 1979).

Based on studies of the Na-K ATPase in red cells, nerve, and in several epithelia, it appears that the hydrolysis of each molecule of ATP is associated with the outward movement of three sodium ions and the inward movement of two potassium ions (Glynn and Karlish, 1975; Nielsen, 1979; Kirk et al., 1980). Accordingly, a metabolically driven potassium pump has been included in the lateral cell membrane, transporting at a rate that is two-thirds of the active sodium flux. This creates a large, potassium influx into the cell and poses somewhat of a problem for selecting potassium permeabilities of the cell apical and basolateral membranes. If one considers an intracellular potassium concentration of 135 meq/liter (Thurau et al., 1981) and an intracellular potential of −74 mV (Fromter et al., 1971), or as in the present model calculations, 141 meq/liter and −73 mV, then relative to a peritubular bath with 5 meq/liter potassium, the electrochemical driving force for potassium out of the cell is 1.1 or 1.3 J/mmol. These are comparable with the driving force of 1.6 J/mmol obtained recently by Cemerikic et al. (1982) using K-selective microelectrodes. If potassium exit back across the basolateral membrane were entirely diffusive and amounted to 5×10^{-6} mmol/cm^{2}s (half the net sodium flux), then, using the model parameters, the thermodynamic permeability coefficient for potassium would be 3.8×10^{-6} (mmol)^2/J · s · cm^2. Using Eq. 19, this corresponds to an

TABLE I
PARAMETER VALUES

Constants
RT = 1.9×10^4 mm Hg · cm^3/mmol
= 2.5 J/mmol
F = 96.5 C/meq
pK_C = 6.1
pK_P = 6.8
pK_B = 7.5

Dimensions and impermeant species concentrations

Apical cell membrane area (A_{MI})	45 cm^2/cm^2 epithelium
Tight junction area (A_{ME})	1.85×10^{-4} cm^2/cm^2 epithelium
Cell perimeter (S)	3.6×10^4 cm/cm^2 epithelium
Cell height (L)cm	$L = 0.0012\,[1 + 0.8(P_I - P_M)]$

Channel basement membrane area (A_{ES}) cm^2/cm^2 epithelium
$A_{ES} = 0.011\,[1 + 0.13(P_E - P_I)]$
Channel volume (V_E) cm^3/cm^2 epithelium

$$V_E = \frac{L}{4}\,[A_{ME} + 20 \cdot A_{ES} + A_{ES}]$$

Reference cell volume (V_I°)	0.0012 cm^3/cm^2 epithelium
Reference impermeant species concentration* (C_I°)	40 mOsM/liter
Reference total cell buffer concentration* (C_{Buf}° + C_{HBuf}°)	60 mmol/liter

Membrane properties

	channel tight junction	channel basement membrane	cell apical membrane	cell basolateral membrane
	L_P	*cm/s · mm Hg*		
	2.0×10^{-3}	2.0×10^{-4}	2.0×10^{-8}	2.0×10^{-8}
	Reflection coefficient, σ			
Na	0.75	0.00	1.0	1.0
K	0.75	0.00	1.0	1.0
Cl	0.30	0.00	1.0	1.0
HCO_3	0.90	0.00	1.0	1.0
HPO_4	0.90	0.00	1.0	1.0
H_2PO_4	0.90	0.00	1.0	1.0
H	0.20	0.00	1.0	1.0
	Thermodynamic straight coefficients L_{ii} (mmol)^2/J · s · cm^2			
Na	5.0×10^{-2}	4.0×10^{-3}	4.0×10^{-8}	2.0×10^{-9}
K	2.0×10^{-3}	1.0×10^{-4}	1.0×10^{-8}	3.0×10^{-8}
Cl	4.0×10^{-2}	4.0×10^{-3}	1.8×10^{-8}	1.8×10^{-8}
HCO_3	2.0×10^{-3}	2.0×10^{-3}	5.0×10^{-10}	1.2×10^{-8}
HPO_4	1.0×10^{-4}	2.0×10^{-4}	8.0×10^{-11}	1.0×10^{-10}
H_2PO_4	1.0×10^{-4}	2.0×10^{-4}	1.0×10^{-9}	4.0×10^{-10}
H	1.0×10^{-3}	2.0×10^{-3}	2.7×10^{-8}	4.0×10^{-10}

Degrees of coupling

Apical membrane
$q_{13} = 0.60$ (Na—Cl)
$q_{16} = 0.25$ (Na—H_2PO_4)
$q_{17} = -0.70$ (Na—H)
Basolateral membrane
$q_{23} = 0.70$ (K—Cl)

Sodium-potassium pump at the basolateral membrane
$J_1^{act} = 6.0 \times 10^{-4}\,[C_{1I} - 0.008]$ mmol/s · cm^2
$J_2^{act} = -0.67\,J_1^{act}$

*Actual impermeant concentrations are computed according to $C_I = (V_I^\circ/V_I)\,C_I^\circ$.

electrical resistance of 28 Ωcm^2 indicating a pathway four times more conductive than the total electrical conductivity of the membrane (Fromter, 1979). Exit across the apical membrane cannot be important since the resistance here is roughly three times that of the peritubular membrane (Fromter, 1979). A particularly convenient solution to this problem of potassium exit is the possibility of coupled K-Cl exit across the basolateral membrane. This will now be considered in relation to chloride transport.

Evidence suggests that in the rat proximal tubule there is substantial transcellular chloride flux and that this chloride enters the cell across the luminal membrane in association with sodium. Such NaCl cotransport has been clearly demonstrated in gastrointestinal epithelia (Frizzell et al., 1979) and in the proximal tubule of *Necturus* by Spring and Kimura (1978). In the rat there is substantial NaCl reabsorption when the lumen contains a high chloride, bicarbonate-depleted solution (Green and Giebisch, 1975*a*), and two-thirds of this flux may be inhibited by the luminal application of furosemide (Lucci and Warnock, 1979). Given these observations, luminal membrane chloride permeability and coupling coefficient to sodium have been selected to achieve the desired reabsorptive chloride flux. The problem of basolateral chloride exit involves considerations similar to those for potassium. For a cellular chloride concentration of 35 mM, a peritubular concentration of 113 mM, and a cell electrical potential of -74 mV, there is a driving force for chloride across the basolateral membrane of 4.1 J/mmol. To obtain a flux of 5×10^{-6} mmol/s · cm^2 (half the net sodium flux) across this membrane requires a straight permeability coefficient of 1.2×10^{-6} $(mmol)^2/J \cdot s \cdot cm^2$ or a partial conductance of 89 Ωcm^2. As indicated above, this is comparable with the total conductance of this membrane. However, in ion substitution experiments no appreciable chloride conductance is found (Fromter, 1974). The existence of basolateral K-Cl cotransport, as has been posited for gallbladder (Reuss, 1979; Gunter-Smith and Schultz, 1982), can provide a mechanism for electrically silent chloride exit and has been incorporated into this model. Chloride-bicarbonate countertransport would appear to be energetically unfavorable for chloride exit (Table II).

The presence of a Na^+/H^+ countertransport system in the apical membrane of the rat proximal tubule was securely established by Murer et al. (1976) using a suspension of vesicles prepared from this membrane. Such countertransport has been confirmed in the rabbit proximal tubule by the vesicle experiments of Kinsella and Aronson (1980). In both preparations the Na^+/H^+ exchange is an electroneutral process, indicating one-to-one stoichiometry. Note that the thermodynamic coefficients selected for the apical membrane in this model represent an amalgam of several parallel pathways for sodium through the membrane. As such, the net coupling of sodium to proton flux may be far from complete. In their micropuncture experiments in the rat proximal tubule, Green and Giebisch (1975*b*) have indicated maneuvers that can substantially change the coupling of these fluxes. The model parameters have been chosen so as to achieve the desired net luminal acidification rate, a neutral cell pH (Khuri, 1979), and substantial bicarbonate permeability of the basolateral cell membrane (Fromter and Sato, 1976). A baseline pCO_2 of 50 mm Hg has been used in accordance with the data of Gennari et al. (1982).

The coupling of Na^+ to $H_2PO_4^-$ at the apical cell membrane has been suggested by Bank et al. (1974), and has been incorporated into this model. The magnitude of the coefficients at apical and basolateral membranes was selected to obtain reasonable cell phosphate concentrations and a phosphate to sodium net flux ratio comparable with their luminal concentrations (Sutton et al., 1979). It may be verified in Table I that for the coupled fluxes at the apical cell membrane $q_3^2 + q_6^2 + q_7^2 = 0.91$, so that the proposition of the previous section guarantees that this is a thermodynamically passive structure.

There is little guidance from the literature in the choice of permeabilities for the components of the paracellular pathway, tight junction and channel basement membrane. There is, presumably, no ion–ion coupling at either of these structures, so that the permeability selection is essentially a choice of partial conductance for each species. The total resistance of the tight junction is of the order of 5 Ωcm^2 (Fromter, 1979) and this was taken as a constraint on the model parameters. The resistance of the channel basement membrane was assumed to be ~ 1 Ωcm^2, which gave reasonable agreement with the net water permeability of the epithelium. (The effect of basement membrane solute permeability on epithelial water permeability will be considered in the last section.)

The numerical methods used in solving the model equations were those described in detail by Stephenson (1978) for kidney models, and used previously in the solution of epithelial problems (Weinstein and Stephenson, 1979). For time-dependent problems the derivatives were represented by a finite difference scheme centered in time. The nonlinear finite difference equations were then solved iteratively using Newton's method. The problems were coded in FORTRAN, running under the RT-11 operating system, on a PDP/11/23 processor (Digital Equipment Corp., Marlboro, MA) with 256 kilobytes of memory. A single, steady state problem required ~ 1 min of central processing unit (CPU) time for solution.

STEADY STATE OPEN-CIRCUITED EPITHELIUM

Table II displays the solution of the model equations for the open-circuited epithelium bathed by equal, Ringer-like solutions. The concentrations and potentials within each compartment are listed in the Intensive variables section of Table II. The open circuit potential of 1 mV is in agreement with that found by Fromter and Sato (1976) and is a

TABLE II

SOLUTION OF THE MODEL EQUATIONS FOR THE OPEN-CIRCUITED EPITHELIUM BETWEEN EQUAL RINGER'S SOLUTION MEDIA (PCO_2 = 50 mm Hg)

Intensive variables	ψ_M	ψ_E	*mV*	ψ_I	ψ_S
	1.0	0.21		−73.4	0.0
	P_M	P_E	*mm Hg*	P_I	P_S
	0.0	9.0		0.1	0.0
	C_M	C_E	*mmol/liter*	C_I	C_S
Na	140.0	142.9		23.1	140.0
K	4.9	4.0		140.9	4.9
Cl	113.0	114.1		38.9	113.0
HCO_3	25.0	25.7		25.3	25.0
HPO_4	3.0	3.1		13.9	3.0
H_2PO_4	0.9	0.9		4.1	0.9
pH	7.32		7.33	7.33	7.32
C_{Buf}	—	—		25.5	—
C_{HBuf}	—	—		38.0	—
C_I	—	—		42.3	—
Osmolality	286.8	290.8		288.5	286.8
	$\mu_M - \mu_S$	$\mu_E - \mu_S$	*J/mmol*	$\mu_I - \mu_S$	
Na	0.10	0.073		−11.58	
K	0.10	−0.50		1.29	
Cl	−0.10	0.0035		4.43	
HCO_3	−0.10	0.051		7.12	
HPO_4	−0.20	0.042		17.98	
H_2PO_4	−0.10	−0.0034		10.87	
H	0.10	−0.051		−7.12	

Fluxes

	J_{vME}	J_{vMI}	J_{vIE}	J_{vES}	J_{vIS}
			nl/s · cm²		
	14.7	28.3	29.0	43.6	−0.6
	J_{ME}	J_{MI}	J_{IE}	J_{ES}	J_{IS}
			nmol/s · cm²		
Na	0.74	8.95	8.96	9.70	0.23×10^{-2}
K	0.24	−0.54	−0.65	−0.41	0.11
Cl	0.42	4.79	4.69	5.12	0.10
HCO_3	−0.018	−0.16	3.66	2.35	0.085
HPO_4	0.12×10^{-3}	−0.065	0.078	0.23	0.18×10^{-2}
H_2PO_4	-0.41×10^{-3}	0.34	0.19	0.031	0.43×10^{-2}
H	0.027	−4.18	−0.12	−1.24	-0.28×10^{-2}
			μamp/cm²		
Current	58.1	−58.1	27.3	85.4	−85.4

Free energy changes at the apical and lateral cell membranes

	Φ_{MI}	Φ_{IE}
	erg/s	
Volume	1.2	1.3
Na	1,045	−1,043
K	6.4	−11.5
Cl	−217	208
HCO_3	11.7	259
HPO_4	11.9	13.9
H_2PO_4	−37.0	20.4
H	−302	8.6
Total	521	−544

consequence of the negative current across the apical cell membrane (Table II, Fluxes section). At this membrane, the extensive coupling of sodium to anions and to proton countertransport permits a positive inward sodium flux to establish a net outward current. Although the water transporting properties of this model will be considered in detail in the following section, note that the model predicts that the cell is only 1.7 mOsM/liter hypertonic and the interspace 4.0 mOsM/liter hypertonic to the lumen. Neither of these values is experimentally discernible, but they are, nevertheless, sufficient to drive the large water flow across this epithelium.

The electrochemical potentials of the solutes with respect to the peritubular solution are indicated in the Intensive variables section of Table II. Within the cell, no ion species is at its equilibrium potential. Due to active transport at the basolateral membrane, the intracellular sodium is in a deep potential well, and the sodium-proton exchange at the apical cell membrane creates a potential well for protons within the cell. Due to the uniform pCO_2 within the system and the reaction equilibrium of protons with bicarbonate, the elevation of bicarbonate above its equilibrium potential is equal and opposite in sign to the lowered proton potential. Similarly, the sum of proton and basic phosphate potentials is equal to that for acid phosphate. Because of the coupled apical entry, the chloride and phosphate are also above equilibrium. In the case of potassium, the potential reflects the balance of metabolically driven input at the basolateral membrane plus the accelerated efflux at this membrane by coupled chloride transport. In this model the balance is a positive potassium potential, and is in agreement with microelectrode observations (Cemerikic et al., 1982).

The free energy changes at the cell apical and lateral membranes have also been indicated in Table II. The energy dissipation at the tight junction, channel basement membrane, and cell basal membrane are all small, with a total contribution of only 23 erg/s. The major loss of free energy in the system occurs at the cell apical membrane with the influx of sodium across a large potential difference. Here some of this energy is recovered with the uphill transport of chloride, phosphate and protons, all showing negative dissipation. Of course, the total dissipation for this membrane is positive. At the lateral membrane, the metabolic energy input is 1,163 erg/s. Most of this, 1,055 erg/s, appears as uphill sodium transport, while the remainder derives from the potassium flux up its small potential gradient into the cell. The figures for sodium and potassium dissipation, which appear in the table, $-1{,}043$ and -11.5 erg/s, reflect both the energy input and the back diffusion of these ions across the lateral membrane. The major dissipative energy losses at this membrane are associated with the efflux of chloride and bicarbonate.

Within the first five significant figures, the energy input from the Na-K exchanger balances the energy dissipation from passive membrane fluxes. When the energy input from mass entry into the system is included, 0.018 erg/s, then energy balance is verified to within the limits of machine accuracy (0.3×10^{-13} erg/s). The total energy expenditure, 1,163 erg/s or 0.28×10^{-4}cal/s, may be referred to the net sodium transport of 9.4 neq/s, so that the cost of transport is 3.0 cal/meq. This figure may be related to some of the known metabolic parameters of proximal tubule. The changes in renal oxygen consumption with respect to changes in sodium transport have given an estimate of 20–30 meq of sodium transported for each millimole of O_2 utilized (Cohen and Kamm, 1981). A P/O_2 ratio of 6 and an energy of hydrolysis for ATP of 14 cal/mmol (Veech et al., 1979) translates into 2.8–4.2 calories available for each milliequivalent of sodium to be absorbed. The concordance of this estimate with the computed dissipation is reassuring, but also suggests the requirement of efficient metabolic energy transduction by the Na/K ATPase.

Table III shows a comparison of some epithelial permeabilities measured for the rat proximal tubule with those determined for the model. The L_p for the model epithelium was computed using the open-circuit preparation with the addition of 1 meq/liter of an impermeant species into the luminal solution. The ionic reflection coefficients and ionic

TABLE III
COMPARISON OF TRANSEPITHELIAL FLUXES AND PERMEABILITIES OF RAT PROXIMAL TUBULE WITH THOSE ACHIEVED BY THE MODEL

	Rat	Model
Fluxes		
	neq/s · cm²	
Na	9.4*	9.7
Cl	5.1*	5.1
HCO_3	2.65*	3.6
RTL_p	*ml/s · cm² OsM × 10⁴*	
	43.6‡	45.4
Reflection coefficient (σ_i)		
Na	0.7§	0.70
Cl	0.43§	0.44
HCO_3	1.0§	0.88
Permeability (P_i)	*cm/s × 10⁵*	
Na	24.7§	16
K	27.1§	24
Cl	21.2§	29
HCO_3	6.7§	4.2
Electrical resistance	*Ωcm²*	
Total	5‖	6.7
Tight junction		6.8
Apical cell membrane	260‖	196
Basolateral cell membrane	90‖	77

*Values as given in the work of Windhager (1979).
‡Values as given in the work of Giebisch and Windhager (1973).
§Values as given in the work of Ullrich (1973).
‖Values as given in the work of Fromter (1979).

permeabilities were computed using the short-circuited epithelial model. Here, for example, 1 meq/liter of sodium with 1 meq/liter of an impermeant species added to the luminal solution could be compared with the effect of adding 1 meq of the impermeant species alone. By subtraction, this yields values for $\Delta J_v/\Delta C_{1M}$ and $\Delta J_1/\Delta C_{1M}$, the changes in volume and sodium flux with changes in the mucosal sodium concentration. The reflection coefficient for sodium is thus

$$\sigma_1 = \frac{1}{L_p}\frac{\Delta J_v}{\Delta C_{1M}} \tag{26}$$

and the sodium permeability is computed by

$$P_1 = \frac{\Delta J_1}{\Delta C_{1M}} - (1 - \sigma_1)C_1\frac{\Delta J_v}{\Delta C_{1M}}. \tag{27}$$

Here Eq. 27 assumes that $\Delta J_1^{act}/\Delta C_{1M}$, the change in metabolically driven sodium transport produced by a change in luminal sodium, is relatively small. The analagous computations were done for K^+, Cl^-, and HCO_3^-, both for increments and decrements of 1 meq/liter; the two permeabilities were averaged and recorded in Table III. The electrical resistance determinations of the epithelium and its individual membranes are the only nonsteady state calculations of this section. For these experiments the epithelium is resting at short circuit at $t = 0$, when a step increase or decrease of 10 mV is made in the transepithelial potential. The time-dependent system of model equations is then solved for time increments of 2 ms, and the changes in transmembrane currents and potentials at $t = 6$ ms are used to compute the individual membrane resistances.

One of the important uses of a model, such as this, where all the intraepithelial fluxes and concentrations are known, is the scrutiny of the predictions of simpler representations of epithelial function. One such formulation, used by Fromter et al. (1973) in their elegant studies of rat proximal tubule, is the elimination of the coupled solute fluxes from Eq. 16

$$J_i = (1 - \sigma_i)\bar{C}_i J_v + \frac{P_i\bar{C}_i}{RT}\Delta\mu_i + J_i^{act} \tag{28}$$

or

$$J_i = J_i^c + J_i^d + J_i^{act}. \tag{29}$$

Here the solute flux is represented as a sum of convective, diffusive, and active transport terms. If we use the constants determined in Table III for the model epithelium to analyze the open-circuit fluxes, we obtain for J_i^c, J_i^d, and J_i^{act} 1.8, 0.9, and 7.0 neq/s · cm^2 in the case of sodium and 2.8, −1.3, and 3.6 neq/s · cm^2 in the case of chloride. With reference to the actual fluxes in Table II, we find that the transjunctional fluxes, J_{ME}, and transcellular fluxes, J_{IE}, are 0.7 and 9.0 for sodium and 0.4 and 4.7 for chloride. It appears, therefore, that the omission of the cross coefficients from Eq. 16 in this case has caused a substantial underestimate of the active transport of sodium and chloride and overestimate of the passive fluxes.

WATER TRANSPORT

A program for the systematic exploration of the water transporting properties of a model epithelium has previously been outlined and applied to transport across nonacidifying gallbladder epithelia (Weinstein et al., 1981). In this scheme, volume and solute transport (mOsM/s · cm^2) are viewed as functions of the mucosal and serosal osmolality

$$\begin{aligned} J_v &= J_v(C_M, C_S; C_0) \\ J_s &= J_s(C_M, C_S; C_0). \end{aligned} \tag{30}$$

Here C_0 is a reference osmolality, and C_M and C_S represent deviations of luminal and peritubular solutions from the reference.

The reabsorbate concentration, C_R, is defined by

$$C_R(C_M, C_S; C_0) = \frac{J_s}{J_v} \tag{31}$$

and is the osmolality of the solution transported by the epithelium. When identical media bathe the tissue ($C_M = C_S = 0$), a useful measure of intraepithelial solute-solvent coupling may be defined by

$$\gamma = \frac{C_0}{C_R(0, 0; C_0)} = \frac{J_v}{J_s/C_0}. \tag{32}$$

Eq. 32 indicates that the osmotic coupling coefficient, γ, is equal to the observed volume flow in the absence of external forces, relative to the volume flow required to achieve transport at the reference osmolality.

In the proximal tubule, osmotic transport equilibrium is achieved when the osmolality of the transported solution is equal to the osmolality of the luminal contents. This equality may be represented by

$$C_0 - C_M^* = C_R(-C_M^*, 0; C_0). \tag{33}$$

The left-hand side of Eq. 33 is the luminal osmolality, and C_M^* is the deviation from reference at which transport equilibrium has occurred. The right-hand side indicates that the reabsorbate osmolality is to be evaluated with the serosal solution at the reference osmolality. A known, unaltered peritubular osmolality would be a legitimate assumption, for example, for an isolated perfused proximal tubule or for a microperfused segment of proximal tubule with its relatively large capillary blood flow. At osmotic transport equilibrium the lumen will continue to be depleted of solutes and water, but its osmolality will remain unaltered. An analogous osmotic transport equilibrium may be calculated for the increment in serosal osmolality,

which results in equality with the transported solution

$$C_0 + C_S^* = C_R(0, C_S^*; C_0). \quad (34)$$

This condition may be found in experimental maneuvers in which the peritubular solution is small in volume and, in fact, generated by the reabsorbate (Barfuss and Schafer, 1981). When both C_M^* and C_S^* are small, relative to the reference osmolality; the epithelium is said to transport water isotonically.

The characterization of water transport must also include the capability of the epithelium to transport water against an adverse osmotic gradient. The gradient that just brings water transport to a halt is termed the "strength of transport." This is denoted by $\hat{C}$, and is specified as the solution to the equation

$$J_v(\hat{C}, 0; C_0) = 0. \quad (35)$$

From very general considerations (Weinstein et al., 1981) it can be shown that if an epithelium is capable of both isotonic transport and transport against a significant osmotic gradient, then intraepithelial coupled water transport must be substantial ($\gamma \approx 1$). This is the case, for example, in the rabbit gallbladder epithelium or the rat small intestine. The strength of transport for proximal tubule, is, at present, unknown. Bomsztyk and Wright (1982), however, have reported that in the rat proximal tubule, microperfused with a low bicarbonate solution (10 meq/liter), an additional 30 mmol/liter of mannitol was required in the luminal solution to nullify volume reabsorption. The interpretation of these observations is complicated by the presence of several forces affecting water movement. Water reabsorption is enhanced by the anion asymmetry, perhaps accounting for as much as 9 mOsM/liter, and by capillary blood protein, perhaps as much as 4 mOsM/liter in oncotic pressure (Lewy and Windhager, 1968). It may be the case, therefore, that intraepithelial solute-solvent coupling in the rat proximal tubule provides a strength of transport equal to 17 mmol/liter of mannitol (or 24 mmol/liter of NaCl). This is comparable with the strength of transport of the model epithelium with the reference parameter set (see below).

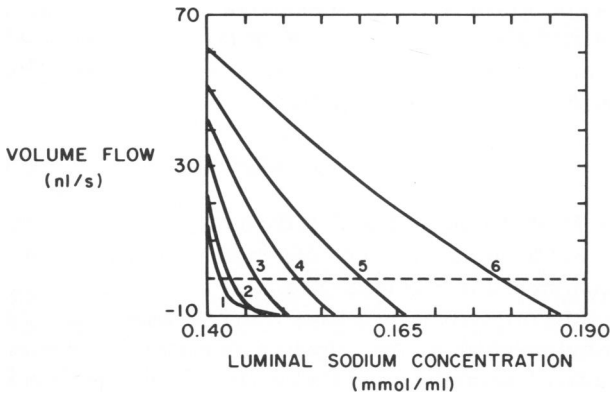

FIGURE 2 Volume transport as a function of luminal sodium: variation of channel basement membrane solute permeability. Each curve corresponds to a set of experiments in which all the basement membrane solute permeabilities have been scaled; 1, reference × 10; 2, reference × 5; 3, reference × 2; 4, reference; 5, reference × 0.5; and 6, reference × 0.2. Luminal sodium is increased by the addition of NaCl; peritubular sodium remains at 0.140 mmol/ml. The intersection of each curve with the line $J_v = 0$ indicates the strength of transport for that model.

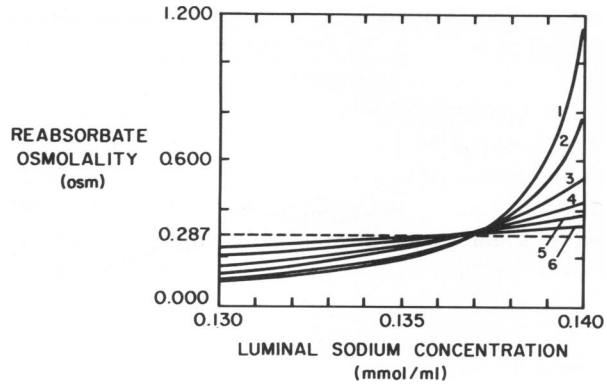

FIGURE 3 Transport tonicity as a function of luminal sodium: variation of channel basement membrane solute permeability. Each curve corresponds to a set of basement membrane solute permeabilities as in Fig. 2. Luminal sodium is decreased by the removal of NaCl; peritubular sodium remains at 0.140 mmol/ml. Mucosal transport equilibrium occurs when the reabsorbate osmolality is equal to the luminal osmolality.

The parametric dependence for these features of water transport has been completely delineated for a nonelectrolyte model of the lateral intercellular space (Weinstein and Stephenson, 1981*a*). Isotonic transport was achieved whenever the cell membranes and tight junction, in parallel, were sufficiently water permeable, and was uninfluenced by channel basement membrane solute permeability. The capability of uphill water transport, by contrast, was solely determined by the degree of solute trapping within the interspace, and predicted by the ratio of solute transport, J_s, relative to channel basement membrane

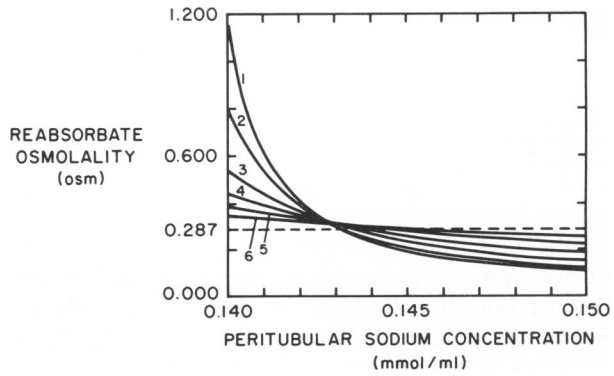

FIGURE 4 Transport tonicity as a function of peritubular sodium: variation of channel basement membrane solute permeability. Each curve corresponds to a set of basement membrane solute permeabilities as in Fig. 2. Peritubular sodium is increased by the addition of NaCl; luminal sodium remains at 0.140 mmol/ml. Serosal transport equilibrium occurs when the reabsorbate osmolality is equal to the peritubular osmolality.

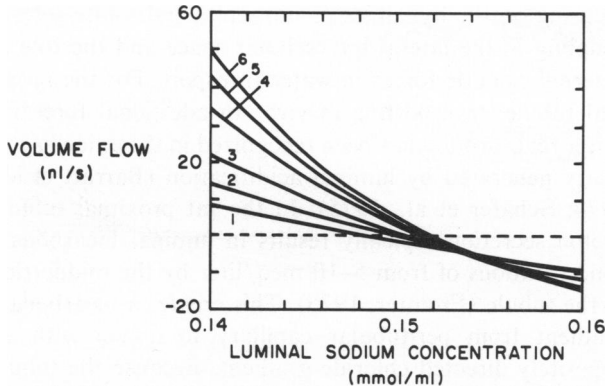

FIGURE 5 Volume transport as a function of luminal sodium: variation of mucosal water permeability. Each curve corresponds to a set of experiments in which the water permeabilities of the tight junction, apical cell membrane and lateral cell membrane have been scaled; 1, reference × 0.05; 2, reference × 0.1; 3, reference × 0.2; 4, reference × 0.5; 5, reference; and 6, reference × 2. Luminal sodium is increased by the addition of NaCl; peritubular sodium remains at 0.140 mmol/ml. The intersection of each curve with the line $J_v = 0$ indicates the strength of transport for that model.

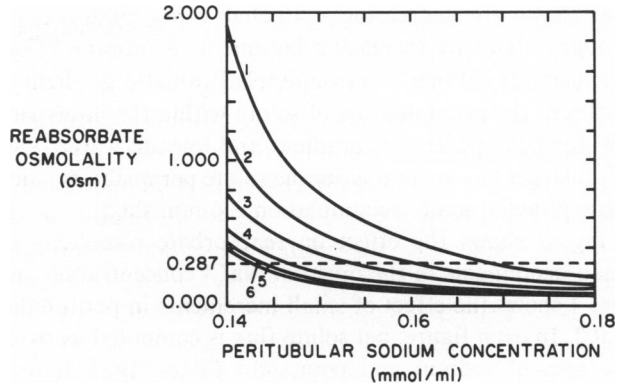

FIGURE 7 Transport tonicity as a function of peritubular sodium: variation of mucosal water permeability. Each curve corresponds to a set of water permeabilities as in Fig. 5. Peritubular sodium is increased by the addition of NaCl; luminal sodium remains at 0.140 mmol/ml. Serosal transport equilibrium occurs when the reabsorbate osmolality is equal to the peritubular osmolality.

solute permeability. The epithelial water permeability, L_p, was found to depend on both parameters, cell membrane water permeability and interspace outlet resistance. Whenever the epithelium was capable of significant uphill water transport, the measured L_p was shown to be an underestimate of the cell membrane water permeability.

Figs. 2–7 and Table IV summarize the results of a series of osmotic experiments using the proximal tubule model. Fig. 2 displays the effect on transepithelial volume flow in six series of steady state experiments in which the luminal NaCl concentration was increased. Each curve corresponds to a different set of values of channel basement membrane solute permeabilities, in which all the thermodynamic coefficients for this membrane were multiplied by a common factor. The reference values are those given in Table I, and the experiments span a 50-fold range of permeabilities. For each of the experiments, as the luminal salt concentration is increased, the net volume flow decreases. The intersection of each curve with the line, $J_v = 0$, gives the strength of transport, $\hat{C}$, for that model, and these are indicated in the upper section of Table IV. As the solute permeability of the channel outlet decreases, the strength of transport increases. The y-intercept of each curve corresponds to the volume flow when the bathing media are identical, and thus, indicates the degree of solute-solvent coupling for each model. As is apparent from Fig. 2 and Table IV, intraepithelial coupling is enhanced by decreased basement membrane permeability. Finally, when these experiments are repeated using an impermeant species the slope of each curve is just the osmotic water permeability of the epithelium. Table IV lists the values of RTL_p determined at the point of identical bathing media

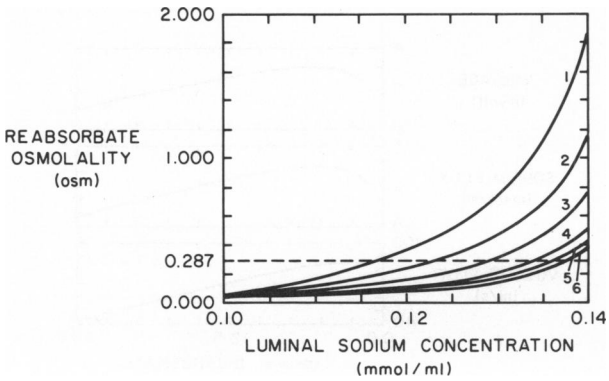

FIGURE 6 Transport tonicity as a function of luminal sodium: variation of mucosal water permeability. Each curve corresponds to a set of water permeabilities as in Fig. 5. Luminal sodium is decreased by removal of NaCl; peritubular sodium remains at 0.140 mmol/ml. Mucosal transport equilibrium occurs when the reabsorbate osmolality is equal to the luminal osmolality.

TABLE IV

EPITHELIAL WATER PERMEABILITY, EQUILIBRIUM OSMOLALITIES, STRENGTH OF TRANSPORT, AND INTRAEPITHELIAL SOLUTE-SOLVENT COUPLING. VARIATION OF CHANNEL BASEMENT MEMBRANE SOLUTE PERMEABILITY AND MUCOSAL WATER PERMEABILITY

	RTL_p	C_M^*	C_S^*	$\hat{C}$	γ
	μl/s · cm² · OsM		*mOsM/liter*		
P_{ES} × 1/5	2.8	9.6	12.1	77.2	0.84
×1/2	3.7	8.3	9.4	40.0	0.75
Reference	4.6	7.4	8.0	23.2	0.66
×2	5.7	6.8	7.1	12.9	0.53
×5	7.0	6.4	6.5	5.7	0.36
×10	7.7	6.2	6.3	3.0	0.24
L_{pM} × 1/20	0.7	47.0	58.0	18.0	0.15
×1/10	1.1	34.4	39.8	20.0	0.25
×1/5	1.9	22.8	25.3	21.3	0.37
×1/2	3.2	12.0	13.0	22.4	0.54
Reference	4.6	7.4	8.0	23.1	0.66
×2	6.3	4.9	5.2	24.2	0.74

and shows the increasing epithelial water permeability brought about by increasing basement membrane solute permeability. When a transepithelial osmotic gradient is imposed, the accumulation of solute within the interspace will tend to oppose this gradient and impede water flow. With larger basement membrane solute permeability, such intraepithelial solute accumulation is diminished.

Fig. 3 shows the effect on reabsorbate osmolality of small decrements in the mucosal NaCl concentration and Fig. 4 shows the effect of small increments in peritubular NaCl. In each figure, net solute flux is computed as twice the sum of sodium and potassium fluxes. Both figures include six curves corresponding to the basement membrane solute permeabilities considered in Fig. 2. For the highest solute permeability the intraepithelial coupling is lowest and the reabsorbate osmolality for identical bathing media exceeds 1 M. Nevertheless, in each figure, the six curves nearly have a common point of intersection, and the attainment of osmotic transport equilibrium is little influenced by the channel basement membrane solute permeability. Table IV indicates the values of the transport equilibria, C_M^* and C_S^*, for each parameter set. For the reference parameter set, luminal transport equilibrium is achieved at an osmotic deviation of 7.4 mOsM/liter, or a decrease in luminal sodium of 3.7 meq/liter. This 2.6% decrease from reference could well have escaped experimental detection, although recently Green and Giebisch (1982) have reported small degrees of luminal hypotonicity in perfused rat proximal tubules.

Between the luman and the lateral intercellular space, water may cross either the tight junction or the apical and lateral cell membranes in series. In Figs. 5–7, the water permeabilities of these "mucosal membranes" have been varied together over a 40-fold range to assess the effect on net water transport. Fig. 5 contains a series of experiments similar to Fig. 2, in which increments in luminal NaCl concentration retard water reabsorption. The figure demonstrates that the strength of transport is little affected by the mucosal water permeability, although examination of the y-intercepts (and reference to Table IV) shows that intraepithelial solute-solvent coupling is enhanced by greater cell membrane water permeability. Similarly, as would be anticipated, whole epithelial, L_p, is increased with greater cell membrane water permeability. Note, however, that the increase in mucosal water permeability by a factor of 40 results in only a ninefold increase in L_p. This reflects the greater influence of solute-solvent coupling within the interspace at the higher cell water permeabilities. Figs. 6 and 7 show the substantial impact of the membrane water permeabilities on the reabsorbate osmolality and the attainment of osmotic transport equilibra. With reference to Table IV, only permeabilities at least as great as in the reference parameter set may be said to be compatible with isotonic transport.

The foregoing discussion has emphasized the similarity of the proximal tubule model to the gallbladder models by focusing on the dynamics of intraepithelial solute-solvent coupling in the lateral intercellular space and the role of external osmotic forces in water transport. For the proximal tubule, transporting in vivo, an additional force for water reabsorption has been recognized in the anion asymmetry generated by luminal acidification (Barratt et al., 1974; Schafer et al., 1975). In the rat proximal tubule, proton secretion typically results in luminal bicarbonate concentrations of from 5–10 meq/liter by the midportion of the tubule (Fromter, 1975). This creates a bicarbonate gradient from peritubular capillary to lumen with an oppositely directed chloride gradient. Because the tubule chloride permeability is greater than that for bicarbonate, the net result is a positive luminal electrical potential, and with it, an enhanced driving force for passive sodium reabsorption. Further, the greater reflection coefficient for bicarbonate results in a significant transepithelial force for water reabsorption. These mechanisms may be demonstrated in this model of rat proximal tubule.

Figs. 8–10 and Table V display the results of a series of steady state experiments in which the luminal solution has been progressively acidified by the addition of HCl. This titrates both bicarbonate and phosphate buffer and the bicarbonate concentration has been indicated on the abcissa. The pCO_2 has been kept at 50 mm Hg and all parameters remain at their reference values (Table I). Fig. 8 shows that for a decrease of bicarbonate concentration from 25 meq/liter to 5 meq/liter there is a progressive increase in luminal electrical potential, sodium reabsorption, and volume flow. Below 5 meq/liter bicarbonate, volume flow increases only slightly and the sodium flux and potential actually decline. This decrease in electrical potential with the most acid luminal solutions reflects an enhanced bicarbonate entry as well as backflux of protons across the tight junction. Fig. 9 contains graphs of the luminal pH and luminal acid flux during these experiments. The curve of net acid entry reflects the balance of proton secretion, proton back-diffusion, and passive bicarbonate

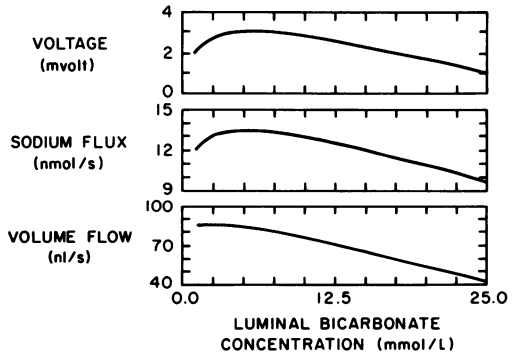

FIGURE 8 Variation of luminal bicarbonate concentration with constant pCO_2 (50 mm Hg): Effect on transepithelial potential difference, sodium flux and volume flow. Luminal bicarbonate concentration has been decreased by titration with HCl; peritubular solutes are at their reference concentrations.

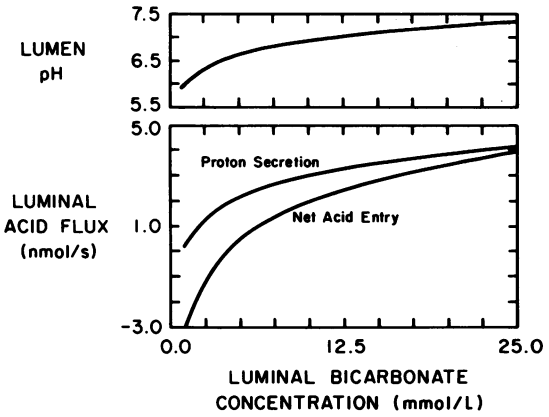

FIGURE 9 Variation of luminal bicarbonate concentration with constant pCO_2 (50 mm Hg): effect on luminal acidification. These are the same experiments indicated in Fig. 8. The graph of proton secretion indicates net proton flux across the cell apical membrane. "Net acid entry" includes proton secretion, proton backflux across the tight junction, and diffusion of bicarbonate into the lumen.

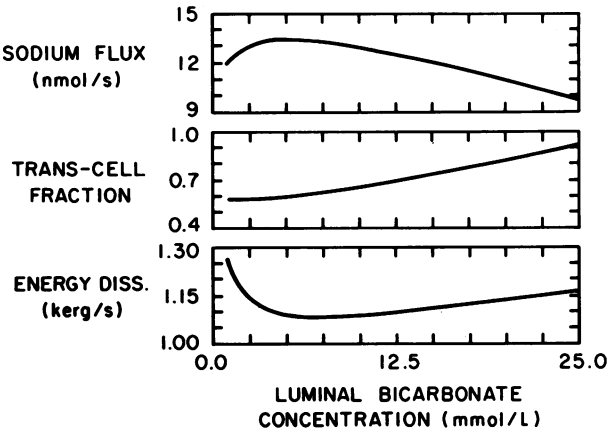

FIGURE 10 Variation of luminal bicarbonate concentration with constant pCO_2 (50 mm Hg): effect on sodium flux and energy dissipation. These are the same experiments as indicated in Fig. 8. *Middle*, the fraction of transepithelial sodium flux that traverses the apical cell membrane. *Bottom*, total energy dissipation of the system.

diffusion into the lumen. Thus, although proton secretion by the apical Na^+/H^+ exchanger continues down to a luminal pH of 6.0, net acid entry ceases at a luminal bicarbonate concentration of 5 meq/liter and a pH of 6.6.

Fig. 10 addresses the effect of luminal acidification on the energetic cost of sodium reabsorption. Between luminal bicarbonate concentrations of 25 meq/liter and 5 meq/liter there is a rise in the net transepithelial sodium flux that is completely attributable to an increase in the passive flux across the tight junction. There is, in fact, a slight decline in the sodium flux across the cell apical membrane due to decreased sodium/proton exchange. Since sodium flux across the apical cell membrane is down a large energy hill, any reduction in this flux will result in decreased energy dissipation for the system (bottom panel). Thus, when the bicarbonate has reached 5 meq/liter, there has been a small decline (6.5%) in the absolute dissipation (Table V). Of more significance, however, is the fact that the transcellular fraction of sodium reabsorption has fallen substantially (from ~90% to 60%) so that the relative cost, in terms of calories per milliequivalent, has similarly fallen. Below 5 meq/liter bicarbonate there is a sharp rise in the total energy dissipation, and this reflects increased dissipation at the tight junction due to bicarbonate and proton diffusion.

It is worth reporting that the experiments of Figs. 8–10 have been repeated with the ambient pCO_2 at 20 and 80 mm Hg. The resulting curves for net transport were virtually superimposable with the figures presented. Chan et al. (1982) have shown, however, that in the perfused rat proximal tubule, luminal acidification is increased with elevation of the ambient pCO_2. The results of these calculations suggest therefore that the observed increase in acidification may be due to an effect of CO_2 that has not been reckoned with in this model. Such an effect could be the incorporation of new apical membrane (with additional sodium-proton exchangers) as seen in turtle urinary bladder (Gluck et al., 1982). More likely, it may be a nonlinear enhancement of apical membrane Na^+/H^+ exchange, which has been reported with cytosolic acidification (Aronson et al., 1982).

This model may also be used to elucidate the changes within the proximal tubule cell in response to luminal acidification, as they occur over time. This is illustrated in Fig. 11 in which the transient responses of several variables have been plotted following an abrupt decrease in luminal bicarbonate from 25 meq/liter to 5 meq/liter (pH 7.32 to 6.62). Note that each panel shows a control, steady state value, followed by a logarithmic time scale permitting display of events from 0.1 to 100 s after the step change in luminal solution. Immediately after the luminal acidification there is net acid entry into the cell across the apical

TABLE V
EFFECT OF LUMINAL ACIDIFICATION ON OPEN CIRCUIT POTENTIAL, NET TRANSPORT, AND ENERGY DISSIPATION

$C_M(HCO_3)$	ψ_M	J_{Na}	J_v	J_H	Φ
mmol/liter	*mV*	*neq/s · cm²*	*nl/s · cm²*	*neq/s · cm²*	*erg/s · cm²*
25	1.0	9.7	43.6	−3.5	1,163
15	2.3	12.0	65.8	−2.5	1,108
5	3.0	13.4	85.3	−0.1	1,087

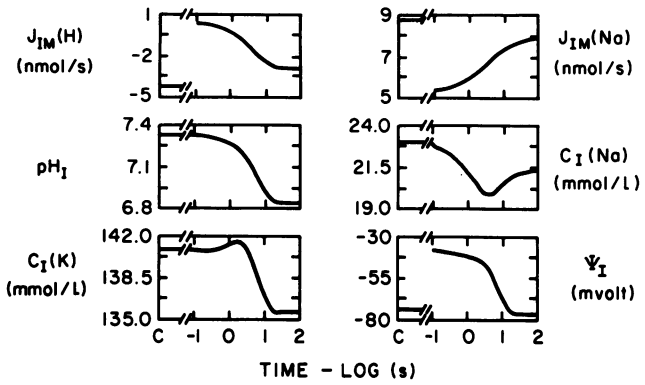

FIGURE 11 Transient response following luminal acidification: apical membrane fluxes, cell ion concentrations, and potential. At $t = 0$ the luminal solution is replaced by one that has been titrated to a bicarbonate concentration of 5 meq/liter (at $pCO_2 = 50$ mm Hg). The abcissa for all six graphs indicates a steady state control period, *C*, when bathing media are equal, and then the experimental time period from 0.1 to 100 s on a logarithmic scale.

membrane and an abrupt fall in sodium reabsorption. Within the first 10 s the cell has been acidified to a pH of 6.92. At this point, acid secretion has resumed and sodium reabsorption has returned to nearly normal. With the transient fall in apical sodium entry, there is a decrease in cell sodium concentration that is partially restored in the time period following the initial 10 s. In the first few seconds, the early loss in cell volume causes a slight rise in the cell potassium concentration. However, with time, the decreased cell sodium results in decreased basolateral potassium uptake that yields a lower steady state cell potassium concentration. Finally, note that examination of the cell potential after the first 10 s of the experiment would lead one to posit an electroneutral Na^+/H^+ exchange process at the apical cell membrane. The early time course, however, reveals a substantial depolarization of the cell by the apical membrane proton gradient.

CONCLUSION

A model of the proximal tubule epithelium of the rat has been formulated in which both the sodium transporting and proton secretory properties of the tubule have been represented. Although this is the first mathematical model to achieve this degree of comprehensiveness, it is, in a sense, the minimal model that can be used to study the important forces that drive luminal solute and water reabsorption. For each of the component membranes of the epithelium, the mass transport equations have been cast according to the formalism of linear nonequilibrium thermodynamics. This has been especially important for the representation of coupled ion fluxes across the luminal membrane of the proximal tubule cell, where the multiplicity of ions coupled to sodium permits an inadvertent introduction of an energy source into the model. The analysis of the matrix of thermodynamic permeability coefficients eliminates this danger, and a simple criterion for a passive membrane has been indicated. Indeed, one result of this investigation is that a plausible model of proximal tubule may be elaborated, whose only energy input is the Na^+/K^+ ATPase at the lateral cell membrane.

With the appropriate choice of parameters, the steady state solution of the model equations shows intracellular concentrations and transepithelial fluxes and permeabilities compatible with the rat proximal tubule. Of interest, the calculated energy dissipation for this model epithelium is consistent with the energy available for transport from the hydrolysis of ATP. In addition, the presence of intraepithelial ion-ion coupling may provide a significant source of error in assigning the active components to the individual ion fluxes, unless this coupling is specifically accounted for in the data analysis.

With the present parameter set, about two-thirds of the observed water transport can be accounted for by intraepithelial solute-solvent coupling, i.e., solute transport into a slightly hypertonic lateral intercellular space. The remaining water flow must be driven by transepithelial driving forces, either luminal hypotonicity and/or anion asymmetry (which together account for ~8 mOsM/liter). In the presence of low luminal bicarbonate, there is, in addition to increased water flow, enhanced reabsorption of sodium across the tight junction. The calculation of the energy dissipation in this case shows a decreased energetic cost for sodium reabsorption and suggests a selective advantage for the presence of a paracellular shunt pathway.

In view of the continuing advancement of microelectrode technology, as well as the study of isolated membrane preparations, this can be considered, at best, a tentative model of the rat proximal tubule epithelium. Nevertheless, although the parameter set may require frequent revision, the underlying mathematical structure of the model should be more durable. This type of model provides a useful, if not necessary, means of integrating a wide variety of experimental observations.

This investigation was supported by U. S. Public Health Service grant 1-RO1-AM-29857-01 from the National Institute of Arthritis, Diabetes, and Digestive and Kidney Diseases.

Received for publication 3 March 1983 and in final form 27 June 1983.

REFERENCES

Aronson, P. S., J. Nee, and M. A. Suhm. 1982. Modifier role of internal H^+ in activating the Na^+/H^+ exchanger in renal microvillus membrane vesicles. *Nature (Lond.).* 299:161–163.

Bank, N., H. S. Aynedjian, and S. W. Weinstein. 1974. A microperfusion study of phosphate reabsorption by the rat proximal renal tubule. *J. Clin. Invest.* 54:1040–1048.

Barfuss, D. W. and J. A. Schafer. 1981. Collection and analysis of absorbate from proximal straight tubules. *Am. J. Physiol.* 241:F597–604.

Barratt, L. J., F. C. Rector, Jr., J. P. Kokko, and D. W. Seldin. 1974. Factors governing the transepithelial potential difference across the proximal tubule of the rat kidney. *J. Clin. Invest.* 53:454–464.

Bishop, J. H. V., R. Green, and S. Thomas. 1979. Free-flow reabsorption of glucose, sodium, osmoles, and water in rat proximal convoluted tubule. *J. Physiol. (Lond.)*. 288:331–351.

Bomsztyk, K., and F. S. Wright. 1982. Effects of transepithelial fluid flux on transepithelial voltage and transport of calcium, sodium, chloride, and potassium by renal proximal tubule. *Kidney Int.* 21:269. (Abstr.)

Cemerikic, D., C. S. Wilcox, and G. Giebisch. 1982. Intracellular potential and K activity in rat kidney proximal tubular cells in acidosis and K depletion. *J. Membr. Biol.* 69:159–165.

Chan, Y.L., B. Biagi, and G. Giebisch. 1982. Control mechanisms of bicarbonate transport across the rat proximal convoluted tubule. *Am. J. Physiol.* 242:F532–543.

Cohen, J. J., and D. E. Kamm. 1981. Renal metabolism: relation to renal function. *In* The Kidney. B. M. Brenner and F. C. Rector, Jr., editors. W. B. Saunders Company, Philadelphia. 144–248.

Essig, A. and S. R. Caplan. 1968. Energetics of active transport processes. *Biophys. J.* 8:1434–1457.

Frizzell, R. A., M. Field, and S. G. Schultz. 1979. Sodium-coupled chloride transport by epithelial tissues. *Am. J. Physiol.* 236:F1–8.

Fromter, E. 1974. Electrophysiology and isotonic fluid absorption of proximal tubules of mammalian kidney. *In* Kidney and Urinary Tract Physiology. K. Thurau, editor. Butterworths and Co. (Publishers) Ltd., London. 6:1–38.

Fromter, E. 1979. Solute transport across epithelia: what can we learn from micropuncture studies on kidney tubules? *J. Physiol. (Lond.)*. 288:1–31.

Fromter, E., and K. Sato. 1976. Electrical events in active H^+/HCO_3^- transport across rat kidney proximal tubular epithelium. *In* Gastric Hydrogen Ion Secretion. D. K. Kasbeker, G. Sachs, and W. S. Rehm, editors. Marcel Dekker, Inc., New York. 382–403.

Fromter, E., C. W. Muller, and T. Wick. 1971. Permeability properties of the proximal tubular epithelium of the rat kidney studied with electrophysiological methods. *In* Electrophysiology of Epithelial Cells. F. K. Schattauer Verlag, Stuttgart-New York. 119–148.

Fromter, E., G. Rumrich, and K. J. Ullrich. 1973. Phenomenologic description of Na^+, Cl^- and HCO_3^- absorption from proximal tubules. *Pfluegers Arch. Eur. J. Physiol.* 343:189–220.

Gennari, F. J., C. R. Ceflisch, C. Johns, D. A. Maddox, and J. J. Cohen. 1982. pCO_2 measurements in surface proximal tubules and peritubular capillaries of the rat kidney. *Am. J. Physiol.* 242:F78–85.

Giebisch, G., and E. E. Windhager. 1973. Electrolyte transport across renal tubular membranes. *In* Handbook of Physiology, Section 8. Renal Physiology. J. Orloff and R. W. Berliner, editors. *Am. Physiol. Soc.*, Washington, DC. 315–376.

Gluck, S., C. Cannon, and Q. Al-Awqati. 1982. Exocytosis regulates urinary acidification in turtle bladder by rapid insertion of H pumps into the luminal membrane. *Proc. Natl. Acad. Sci. USA.* 79:4327–4331.

Glynn, I. M., S. J. D. Karlish. 1975. The sodium pump. *Ann. Rev. Physiol.* 13–55.

Gonzalez, E., P. Carpi-Medina, and G. Whittembury. 1982. Cell osmotic water permeability of isolated rabbit proximal straight tubules. *Am. J. Physiol.* 242:F321–330.

Gottschalk, C. W. 1963. Renal tubular function: lessons from micropuncture. *In* The Harvey Lectures, Series 58. Academic Press, Inc., New York. 99–124.

Green, R., and G. Giebisch. 1975*a*. Ionic requirements of proximal tubular sodium transport. I. Bicarbonate and chloride. *Am. J. Physiol.* 229:1205–1215.

Green, R., and G. Giebisch. 1975*b*. Ionic requirements of proximal tubular sodium transport. II. Hydrogen ion. *Am. J. Physiol.* 229:1216–1226.

Green, R., and G. Giebisch. 1982. Hypertonic fluid reabsorption by the rat renal proximal tubule. *Am. Soc. Neph. Abstr.* 163*a*.

Gunter-Smith, P. J., and S. G. Schultz. 1982. Potassium transport and intracellular potassium activities in rabbit gallbladder. *J. Membr. Biol.* 65:41–47.

Huss, R. E., and D. J. Marsh. 1975. A model of NaCl and water flow through paracellular pathways of renal proximal tubules. *J. Membr. Biol.* 23:305–347.

Huss, R. E., and J. L. Stephenson. 1979. A mathematical model of proximal tubule absorption. *J. Membr. Biol.* 45:377–399.

Khuri, R. N. 1979. The electrochemistry of the nephron. *In* Membrane Transport in Biology. Transport Organs. G. Giebisch, editor. Springer-Verlag, New York. 4A:47–95.

Kinsella, J. L., and P. S. Aronson. 1980. Properties of the $Na^+ - H^+$ exchanger in renal microvillus membrane vesicles. *Am. J. Physiol.* 238:F461–469.

Kirk, K. L., D. R. Halm, and D. C. Dawson. 1980. Active sodium transport by turtle colon via an electrogenic Na-K exchange pump. *Nature (Lond.)*. 287:237–239.

Lewy, J. E., and E. E. Windhager. 1968. Peritubular control of proximal tubular fluid reabsorption in the rat kidney. *Am. J. Physiol.* 214:943–954.

Lucci, M. S., and D. G. Warnock. 1979. Effects of anion-transport inhibitors on NaCl reabsorption in the rat superficial proximal convoluted tubule. *J. Clin. Invest.* 64:570–579.

Macey, R. I. 1979. Transport of water and non-electrolytes across red cell membranes. *In* Membrane Transport in Biology. Transport Across Single Biological Membranes. G. Giebisch, D. C. Tosteson, and H. H. Ussing, editors. Springer-Verlag, New York. 2:1–58.

Morel, F., and Y. Murayama. 1970. Simultaneous measurement of unidirectional and net sodium fluxes in microperfused rat proximal tubules. *Pfluegers Arch. Eur. J. Physiol.* 320:1–23.

Murer, H., U. Hopfer, and R. Kinne. 1976. Sodium/proton antiport in brush-border membrane vesicles isolated from rat small intestine and kidney. Biochem. J. 154:597–604.

Neumann, K. H., and F. C. Rector, Jr. 1976. Mechanism of NaCl and water reabsorption in the proximal convoluted tubule of rat kidney. *J. Clin. Invest.* 58:1110–1118.

Nielsen, R. 1979. A 3 to 2 coupling of the Na-K pump responsible for the transepithelial Na transport in frog skin disclosed by the effect of Ba. *Acta Physiol. Scand.* 107:189–191.

Persson, B., and K. R. Spring. 1982. Gallbladder epithelial cell hydraulic water permeability and volume regulation. *J. Gen. Physiol.* 79:481–505.

Reuss, L. 1979. Electrical properties of the cellular transepithelial pathway in *Necturus* gallbladder III: Ionic permeability of the basolateral cell membrane. *J. Membr. Biol.* 47:239–259.

Sackin, H. and E. L. Boulpaep. 1975. Models for coupling of salt and water transport. *J. Gen. Physiol.* 66:671–733.

Sauer, F. 1973. Nonequilibrium thermodynamics of kidney tubule transport. *In* Handbook of Physiology, Section 8, Renal Physiology. J. Orloff and R. W. Berliner, editors. Am. Physiol. Soc., Washington, DC. 377–398.

Schafer, J. A., C. S. Patlak, and T. E. Andreoli. 1975. A component of fluid absorption linked to passive ion flows in the superficial pars recta. *J. Gen. Physiol.* 66:445–471.

Schafer, J. A., C. S. Patlak, and T. E. Andreoli. 1977. Fluid absorption and active and passive ion flows in the rabbit superficial pars recta. *Am. J. Physiol.* 233:F154–167.

Spring, K. R., and G. Giebisch. 1977. Kinetics of Na^+ transport in Necturus proximal tubule. *J. Gen. Physiol.* 70:307–328.

Spring, K. R., and A. Hope. 1978. Size and shape of the lateral intercellular spaces in the living epithelium. *Science. (Wash. DC).* 200:54–58.

Spring, K. R., and G. Kimura. 1978. Chloride reabsorption by renal proximal tubules of Necturus. *J. Membr. Biol.* 38:233–254.

Spring, K. R., and G. Kimura. 1979. Intracellular ion activities in Necturus proximal tubule. *Fed. Proc.* 38:2729–2732.

Stephenson, J. L. 1978. Analysis of the transient behavior of kidney models. *Bull. Math. Biol.* 40:211–221.

Sutton, R. A. L., G. A. Quamme, and J. H. Dirks. 1979. Transport of calcium, magnesium and inorganic phosphate in the kidney. *In* Mem-

brane Transport in Biology: Transport Organs. G. Giebisch, editor. Springer-Verlag, New York. 4A:357–412.

Thurau, K., F. Beck, J. Mason, A. Dorge, and R. Rick. 1981. Inside the cell–an electron microprobe analysis of the renal tubular electrolyte concentrations. *In* Epithelial Ion and Water Transport. A. D. C. Macknight and J. P. Leader, editors. Raven Press, New York. 137–145.

Ullrich, K. J. 1973. Permeability characteristics of the mammalian nephron. *In* Handbook of Physiology, Section 8, Renal Physiology. J. Orloff and R. W. Berliner, editors. Am. Physiol. Soc., Washington, DC. 377–398.

Veech, R. L., J. W. R. Lawson, N. W. Cornell, and H. A. Krebs. 1979. Cytosolic phosphorylation potential. *J. Biol. Chem.* 254:6538–6547.

Wang, K. W., and W. M. Deen. 1980. Chemical kinetic and diffusional limitations on bicarbonate reabsorption by the proximal tubule. *Biophys. J.* 31:161–182.

Weinstein, A. M., and J. L. Stephenson. 1979. Electrolyte transport across a simple epithelium. Steady-state and transient analysis. *Biophys. J.* 27:165–186.

Weinstein, A. M., and J. L. Stephenson. 1981*a*. Models of coupled salt and water transport across leaky epithelia. *J. Membr. Biol.* 60:1–20.

Weinstein, A. M., and J. L. Stephenson. 1981*b*. Coupled water transport in standing gradient models of the lateral intercellular space. *Biophys. J.* 35:167–191.

Weinstein, A. M., J. L. Stephenson, and K. R. Spring. 1981. The coupled transport of water. *In* Membrane Transport. S. L. Bonting and J. J. H. H. M. de Pont, editors. Elsevier/North Holland Biomedical Press, Amsterdam, New York, and Oxford. 311–351.

Welling, L. W., and J. J. Grantham. 1972. Physical properties of isolated perfused renal tubules and tubular basement membranes. *J. Clin. Invest.* 51:1063–1075.

Welling, L. W., and D. J. Welling. 1975. Surface areas of brush border and lateral cell walls in the rabbit proximal nephron. *Kidney Int.* 8:343–348.

Windhager, E. E. 1979. Sodium chloride transport. *In* Membrane Transport in Biology: Transport Organs. G. Giebisch, editor. Springer-Verlag, New York. 4A:145–213.

Windhager, E. E., G. Whittembury, D. E. Oken, H. J. Schatzmann, and A. K. Solomon. 1959. Single proximal tubules of Necturus kidney. III. Dependence of H_2O movement on NaCl concentration. *Am. J. Physiol.* 197:313–318.